Journal of Hydrology 523 (2015) 24–33

Contents lists available at ScienceDirect

Journal of Hydrology

journal homepage: www.elsevier.com/locate/jhydrol

Periodic seepage face formation and water pressure distribution along a vertical boundary of an aquifer

Seyed Mohammad Hossein Jazayeri Shoushtari [a,*], Peter Nielsen [b], Nick Cartwright [a], Pierre Perrochet [c]

[a] Griffith School of Engineering, Gold Coast Campus, Griffith University, Queensland 4222, Australia
[b] School of Civil Engineering, The University of Queensland, 4072, Australia
[c] Centre d'hydrogéologie, Rue Emile-Argand 11, Case postale 158, 2009 Neuchâtel, Switzerland

ARTICLE INFO

Article history:
Received 24 October 2014
Received in revised form 9 January 2015
Accepted 10 January 2015
Available online 20 January 2015
This manuscript was handled by Corrado Corradini, Editor-in-Chief, with the assistance of Aldo Fiori, Associate Editor

Keywords:
Groundwater
Seepage face
Capillary fringe
Richards' equation

SUMMARY

Detailed measurements of the piezometric head from sand flume experiments of an idealised coastal aquifer forced by a simple harmonic boundary condition across a vertical boundary are presented. The measurements focus on the pore pressures very close to the interface ($x = 0.01$ m) and throw light on the details of the boundary condition, particularly with respect to meniscus suction and seepage face formation during the falling tide. Between the low and the mean water level, the response is consistent with meniscus suction free models in terms of both the vertical mean head and oscillation amplitude profiles and is consistent with the observation that this area of the interface was generally within the seepage face. Above the mean water level, the influence of meniscus formation is significant with the mean pressure head being less than that predicted by capillary free theory and oscillation amplitudes decaying faster than predicted by suction free models. The reduced hydraulic conductivity in this area due to partial drainage of pores on the falling tide also causes a delay in the response to the rising tide. The combined influence of seepage face formation, meniscus suction and reduced hydraulic conductivity generate higher harmonics with amplitudes of up to 26% of the local main harmonic. To model the influence of seepage face formation and meniscus suction a numerical solution of the Richards' equation was developed and evaluated against the data. The model-data comparison shows a good agreement with the behaviour high above the water table sensitive to the choice of moisture retention parameters.

1. Introduction

The interaction between surface and sub-surface water plays an important role in a variety of coastal zone processes including salt-water intrusion and contaminant transport in coastal aquifers (e.g. Cartwright et al., 2004a,b; Cartwright and Nielsen, 2001a,b, 2013; Isla and Bujalesky, 2005; Nielsen, 1999; Nielsen and Voisey, 1998; Robinson et al., 2006; Turner and Acworth, 2004; Xin et al., 2010) and beach profile morphology (e.g. Emery and Foster, 1948; Grant, 1946, 1948). Oceanic forcing of coastal aquifers across the beach face is highly dynamic occurring over a wide range of magnitude and frequency scales (i.e. tide, wave, storm surge, etc.). A number of oceanic and atmospheric mechanisms which have been involved with observed beach water table fluctuations identified by Turner (1998). The majority of studies have described beach groundwater fluctuations due to tidal forces (e.g. Emery and Foster, 1948; Ericksen, 1970; Lanyon et al., 1982; Nielsen, 1990; Turner, 1993a; Turner et al., 1997). A limited number of studies have observed wave-induced the beach water table oscillations (e.g. Bradshaw, 1974; Cartwright et al., 2002, 2006; Hegge and Masselink, 1991; Kang et al., 1994; Lewandowski and Zeidler, 1978; Turner and Nielsen, 1997; Turner and Masselink, 1998; Waddell, 1973, 1976, 1980). Understanding the behaviour of this periodic boundary condition is thus important for accurate modelling of coastal groundwater dynamics and associated issues.

Existing analytical models of ground water dynamics are based on the one or two-dimensional solution of the Boussinesq equation under the Dupuit–Forchheimer assumption, (e.g. Baird et al., 1998; Li et al., 2002; Nielsen et al., 1997; Nielsen, 1990) with corrections for vertical flow effects and also capillary fringe effects by only considering the additional water mass above the water table (e.g. Barry et al., 1996; Cartwright et al., 2005; Li et al., 2000; Nielsen and Perrochet, 2000; Nielsen and Turner, 2000). None of the analytical models consider unsaturated flow or seepage face and meniscus formation at the boundary.

In the natural system, the interface between surface and groundwater is generally sloping; however, in order to simplify

* Corresponding author. Tel.: +61 (0)755527608.
E-mail address: s.jazayerishoushtari@griffith.edu.au (S.M.H. Jazayeri Shoushtari).

http://dx.doi.org/10.1016/j.jhydrol.2015.01.027
0022-1694/

the problem, a vertical interface is considered here. This paper presents detailed measurements of the piezometric head close to the vertical interface ($x = 0.01$ m) of a non-shallow laboratory aquifer forced by simple harmonic oscillations. The data provides insight into the influence of meniscus suction and seepage face formation in and around the inter-tidal zone. The data is then used to evaluate a 2D vertical numerical model based on the Richards' equation (Richards, 1931) with due consideration of the mixed periodic boundary condition to simulate the formation of the seepage face and meniscus suction.

2. Capillary suction and seepage face formation on the interface

Fig. 1 provides a schematic illustration of the pressure distribution along a beach face when the water table exit point becomes decoupled from the ocean level. Note similar scenarios will exist in systems with periodic forcing of groundwater systems such as tidal rivers and lakes where seiching may occur. When decoupling occurs, two distinct pressure zones become apparent. Below the exit point and above the ocean level (i.e. in the seepage face), the surface has a glassy appearance indicating that the water table is at the surface and that the gauge pressure $p(x, z) = 0$. Above the exit point, the surface has a matt appearance due to the presence of meniscuses and as such $p(x, z) < 0$.

The capillary suction gets stronger with increasing elevation above the water table, but upwards of a certain level this suction will not have a significant effect on water table dynamics due to a lack of connectivity in sand with low moisture content and hence very low permeability. Some a priori insight into vertical and horizontal flow in the capillary fringe might be gained from the steady flow study of Silliman et al. (2002).

Several numerical and experimental studies have been conducted which consider the exit point location and seepage face formation. Turner (1993b, 1995) adapted a numerical model from the governing equations of Dracos (1963) to simulate exit point movement across a saturated beach face. The model is based solely on the force balance on a water particle at the sand surface and neglects the sub-surface pressure distribution. In addition, Turner (1993b, 1995) assumed that, during the decoupled phase, the movement of the exit point is independent of the tide level.

Clement et al. (1994) developed a 2D finite-difference algorithm to solve Richards (1931) variably saturated flow equation for porous media which was then applied to solve steady state and transient seepage face problems. Clement et al. (1994) used three kinds of boundary conditions including Dirichlet boundary condition for nodes with known pressure head, Neumann boundary condition for nodes where the values of normal fluxes are known and a seepage face boundary condition. During simulation of the variably saturated flow, the length of seepage face is unknown until the problem is solved; however, the problem cannot be completely solved unless the length of seepage face is determined. Hence, an iterative process is needed to determine the seepage face length at each time step. Clement et al. (1994) used Cooley (1983) modified version of Neuman (1973) iterative-search procedure which is based on the following. During the first iteration, an initial guess of the location of the exit point (i.e. the length of seepage face) is used to solve the flow equation. Based on the solution's results for pressure head and flow along the boundary, it is possible to understand whether the location of exit point is correct or it needs modification. One of three different conditions may exist. First, the solution gives a zero pressure and a net outflow for all nodes along the seepage face which means that the guessed location of exit point is correct. The nodes above the seepage face are considered as a no-flow boundary condition with negative pressure. Second, if the results show non-zero inflow for some of the nodes along the seepage face which have zero pressure, the height of exit point is overestimated. Third, if some of the nodes above the seepage face which are located on no-flow boundary condition get positive flux, the height of the seepage face is underestimated. The seepage face height is then adjusted as required and the flow equation solved again with the new interface pressure profile. This iterative method is repeated until finding the correct length of the seepage face is produced. This model was later validated by

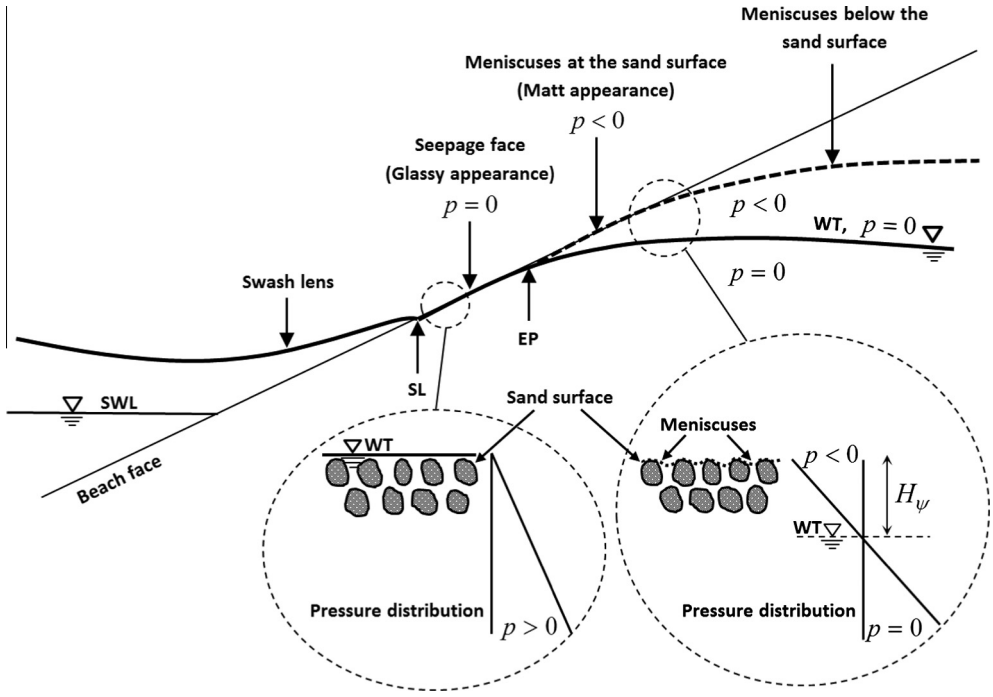

Fig. 1. Schematic illustration of seepage face and meniscuses formation on the beach face. SL = shoreline (swash front); EP = water table exit point; WT = water table; p = pore pressure; H_ψ = steady capillary fringe thickness. Solid and dashed lines represent the free surface and idealised meniscuses surface, respectively (after Cartwright et al., 2006).

Simpson et al. (2003) against laboratory observations in a radial sand tank. Ataie-Ashtiani et al. (1999) also adopted this approach when simulating periodic seepage face formation with the density dependent variably saturated groundwater flow model SUTRA (Voss, 1984).

Li et al. (1997) presented a Boundary Element Method (BEM) model to solve a 2D flow equation to simulate the groundwater fluctuations and seepage face dynamics under tidal forcing for saturated flow conditions using a moving boundary condition. On the water free surface profile (i.e. the water table), the potential head is unknown, but by applying a kinematic boundary condition on the free surface (Liggett and Liu, 1983), the potential head and consequently the water table head elevation profile can be determined. The elevation of the water table exit point can be obtained as the intersection of the water table and beach face profile and the shoreline elevation is the tidal elevation. If the exit point becomes decoupled from the tide then a seepage face exists between shoreline and exit point and the boundary condition on the seepage face is set to atmospheric pressure (i.e. the potential head is equal to elevation head), otherwise, the potential head is calculated based on the tidal elevation.

Baird et al. (1998) developed a numerical solution of the 1D Boussinesq equation including seepage formation. In the numerical model, if the landward computational cell (i.e. cells are located before shoreline) is completely filled with the water, it can be assumed that a seepage face is exist and the most landward cell with this condition will be considered as the exit point. Baird et al. (1998) defined a condition in their numerical Boussinesq model to consider the presence of seepage face. Based on that condition, if at any computational cells the summation of water table elevation and the net rate of groundwater discharge into and out the cell during the time step per cross-shore width of computational cell is greater than the cell's elevation, water level is considered on the ground surface for that cell and decoupling is happened.

3. Experimental setup and procedures

3.1. The flume and sand

The experimental setup is illustrated in Fig. 2 where a 9.2 m long, 0.15 m wide and 1.5 m high unconfined sand flume aquifer is subject to simple harmonic forcing across a vertical boundary at the "ocean" end of the flume and a no-flow boundary condition was used at the "landward" end of the flume. The vertical interface between the external driving head reservoir and the aquifer consisted of a filter made up of stainless steel wire mesh with 0.15 mm openings supported by a coarser grid with 2 cm openings. The top of the flume is open to atmosphere, but it was covered by a loose plastic to minimise any evaporation. To reduce air encapsulation during the sand packing process, the sand was added in ~10 cm thickness layers to the water-filled flume and the layers packed by allowing them to settle by gravity. Subsequent layers where then added and manually mixed with the preceding layer so as to avoid layering due to differential sedimentation.

Locally mined dune sand containing more than 99% quartz content was used in the flume and Table 1 presents the sand's physical and hydraulic properties which were investigated by Nielsen and Perrochet (2000).

3.2. The driving head

The driving head in the clear water reservoir $h_o(t)$, was simple harmonic such that,

$$h_o(t) = d + A_o\cos(\omega t) \tag{1}$$

where d is the mean elevation, A_o is the amplitude and $\omega = 2\pi/T$ is the angular frequency and T is the oscillation period. The data presented here is for the following forcing parameters: $T = 567$ s, $A_o = 0.215$ m and $d = 0.92$ m.

3.3. Monitoring of piezometric head

The piezometric head was measured using UMS-T5 tensiometers installed horizontally into the aquifer through the wall of the flume. The focus of the experiments was on the physics close to the hydrostatic reservoir and so tensiometers were installed at $x = 0.01$ m at each of the following elevations: $z = 0.6, 0.7, 0.8, 0.9, 1.0, 1.1$ m.

4. Numerical modelling

As will be demonstrated later, the experimental observations show significant influence of meniscus suction and seepage face formation on the aquifer response. Neither of these processes are considered by the analytic solutions outlined previously in Section 1 and so a numerical modelling approach was developed.

4.1. Governing equations

To simulate the influence of meniscus formation at the interface above the water table requires consideration of variably saturated flow which is governed by the Richards' equation (Richards, 1931),

$$\left(\frac{C_m}{\rho g} + S_e S\right)\frac{\partial H_p}{\partial t} + \nabla\left(-\frac{\kappa_s}{\mu}k_r(\nabla H_p + \nabla z)\right) = 0 \tag{2}$$

where H_p is the pressure head which is the dependent variable, C_m is the specific moisture capacity, S_e is the effective saturation, S is the storage coefficient, ∇ is the gradient operator, κ_s is the intrinsic permeability which is related to the hydraulic conductivity (K) as

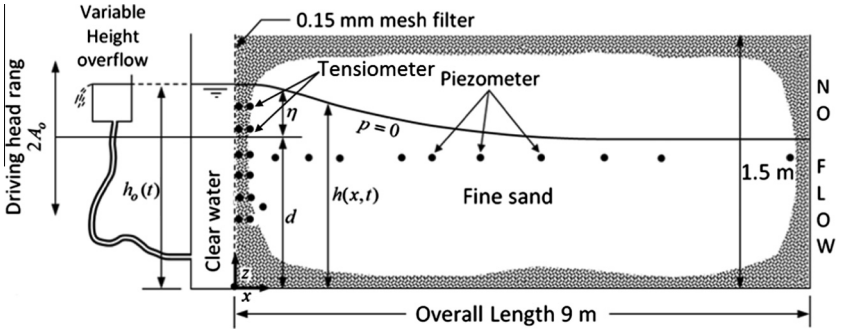

Fig. 2. Schematic illustration of the sand flume (after Cartwright et al., 2003).

Table 1
Hydraulic and moisture properties of the sand.

d_{50} (mm)	K (m/s)	θ_s	θ_r	α (m^{-1})	β	H_ψ (m)
0.260	4.7×10^{-4}	0.41	0.09	1.7	9	0.62

d_{50}, mean grain size; K, saturated hydraulic conductivity; θ_s and θ_r, saturated and residual moisture contents, respectively; H_ψ steady capillary fringe thickness; α and β are van Genuchten parameters. After Nielsen and Perrochet (2000).

$\kappa_s = K\mu/\rho g$, μ is the fluid dynamic viscosity, k_r is the relative permeability, z is the vertical elevation.

Richards' equation (2) is solved here using the finite element method using two commercially available software packages, COMSOL 4.3b (COMSOL, 2013) and FEFLOW 6.0 (FEFLOW, 2012). The two packages were used in order to evaluate differing approaches for modelling seepage face formation as will be described later in Section 4.2.

Solution of Richards' equation (2) requires prior knowledge of the specific moisture capacity C_m and the relative permeability k_r which are both dependent on the soil moisture retention properties. Here, the soil moisture retention properties are quantified using the van Genuchten (1980) formulae,

$$\theta = \begin{cases} \theta_r + \frac{\theta_s - \theta_r}{[1+|\alpha H_p|^\beta]^m} & H_p < 0 \\ \theta_s & H_p \geqslant 0 \end{cases} \tag{3}$$

where θ_r and θ_s are the residual and saturated liquid volume fractions.

The van Genuchten relative permeability is,

$$k_r = \begin{cases} S_e^l \left[1 - \left(1 - S_e^{\frac{1}{m}}\right)\right]^2 & H_p < 0 \\ 1 & H_p \geqslant 0 \end{cases} \tag{4}$$

where the effective saturation is,

$$S_e = \frac{\theta - \theta_r}{\theta_s - \theta_s} \tag{5}$$

The specific moisture capacity is defined as,

$$C_m = \frac{d\theta}{dH_p} = \begin{cases} \frac{\alpha m}{1-m}(\theta_s - \theta_r) S_e^{\frac{1}{m}} \left(1 - S_e^{\frac{1}{m}}\right)^m & H_p < 0 \\ 1 & H_p \geqslant 0 \end{cases} \tag{6}$$

where α, β, $l = 0.5$ and $m = 1 - 1/\beta$ are empirical curve fitting parameters and $H_p = 0$ is the atmospheric pressure distinguishes saturated and unsaturated flow. Table 1 provides hydraulic and moisture parameters of the sand which were used in the numerical simulation.

4.2. Boundary condition implementation

Two different methods were applied to simulate the simple harmonic "ocean" boundary condition with seepage face formation. A Cauchy boundary condition was implemented in the COMSOL simulations and a prescribed head boundary condition combined with flux constraints was used in the FEFLOW simulations. The principle of these two methods is similar to the methods described in 2 i.e. dividing the boundary to three separated parts and changes from Dirichlet to Neumann boundary condition. However, the Cauchy boundary condition uses the logical statements based on the saturation condition and changing the thickness of an artificial layer between external fluid source and the domain to switch between Dirichlet to Neumann boundary condition. The prescribed head with flux constraint method switches the boundary condition between Dirichlet and Neumann based on the flow direction on each part, similar to Clement et al. (1994) method.

4.2.1. Cauchy boundary condition

The Cauchy boundary condition is given by,

$$\mathbf{n}.\rho K \nabla(H_p + z) = \rho R_b \left[(H_{pb} - H_p) + (z_b - z)\right] \tag{7}$$

where H_{pb} and z_b are the pressure and elevation of the distant fluid source, respectively and R_b is the conductance of the material between the source and the model domain. Typically $R_b = K'/B'$, where K' is hydraulic conductivity of the layer and B' is its thickness, which were assumed here to be 4.7×10^{-4} m/s and 0.001 m, respectively.

The Cauchy type boundary condition is used in conjunction with appropriate logical statements in order to switch between a Dirichlet boundary condition for nodes below the ocean level and in the seepage face and a Neumann boundary condition above of the water table exit point (cf. Fig. 3). Following the work of Chui and Freyberg (2009), at the start of each time step, all nodes below the external driving head level (h_o) are assigned pressures assuming a hydrostatic external pressure distribution and for nodes above the driving head level the pressure head is zero,

$$H_{pb} = \begin{cases} h_o - z & \text{for } z \leqslant h_o \\ 0 & \text{for } z > h_o \end{cases} \tag{8}$$

The flow Eq. (2) is then solved and the position of the water table (i.e. $p = 0$) is determined. Below the water table in the saturated zone ($p > 0$) the conductance R_b is modified to a large number ($R_b = K'/B'$) thus creating a flow condition and above the water table the conductance is set to zero ($R_b = 0$) thus creating a no-flow boundary condition. That is,

$$R_b = \begin{cases} \frac{K'}{B'} & \text{for } H_p \geqslant 0 \quad \Rightarrow \quad \text{flow B.C.} \\ 0 & \text{for } H_p < 0 \quad \Rightarrow \quad \text{no-flow B.C.} \end{cases} \tag{9}$$

During the same time step, the new boundary condition (Eq. (9)) is applied and Eq. (2) is solved again and the position of exit point adjusted. This iterative procedure continues until the correct position of the exit point is found such that above the exit point there is no flow and pressure head is negative and that along the seepage face, flow drains the domain and pressure head is zero.

4.2.2. Prescribed head with flux constraint

In the FEFLOW model, seepage face formation is modelled using a prescribed head boundary condition in conjunction with a constrained flux condition. For boundary nodes below the minimum driving head level the head is prescribed to be the same as the driving head (i.e. $h = h_o$ for $z \leqslant \min h_o$). For boundary nodes above the maximum driving head level a no-flow condition is applied (Fig. 4).

For boundary nodes between the minimum and maximum of driving head level the prescribed head with flux constraint is implemented as illustrated in Fig. 5. In each time step, if the driving head level is above the node then the head is prescribed as $h(z) = h_o$ and the flux is unconstrained. If the driving head level is below the node then the node will either be in the seepage face (outflow from the domain) or above the exit point (no-flow). If the flow at the node is positive (i.e. into the domain) then the flux is constrained to $q < 0$ m^3/d and the prescribed head condition is relaxed and the pressure head is allowed to be negative. The model then iterates and adjusts the water table position until the solution converges.

5. Results and discussion

5.1. Piezometric head distribution

Fig. 6 compares the measured and predicted piezometric head time series at different intertidal elevations very close to the boundary, $h^*(x = 0.01\text{ m}, z, t)$. While the driving head is simple

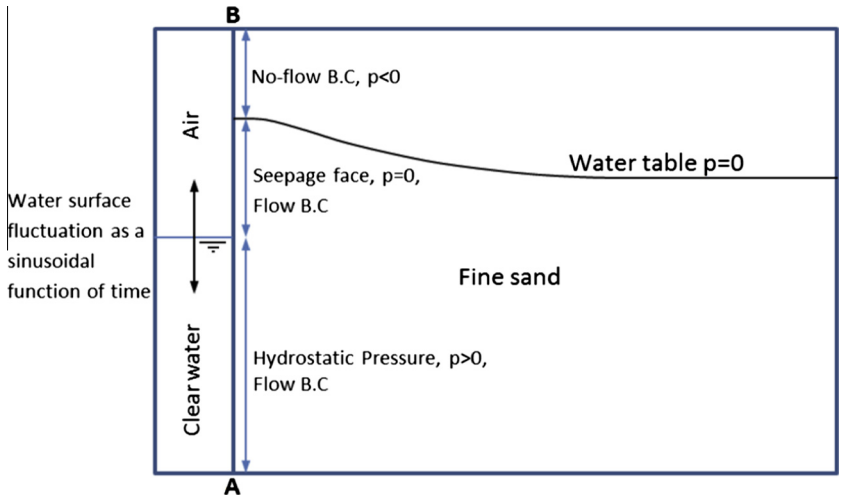

Fig. 3. Periodic Cauchy boundary condition.

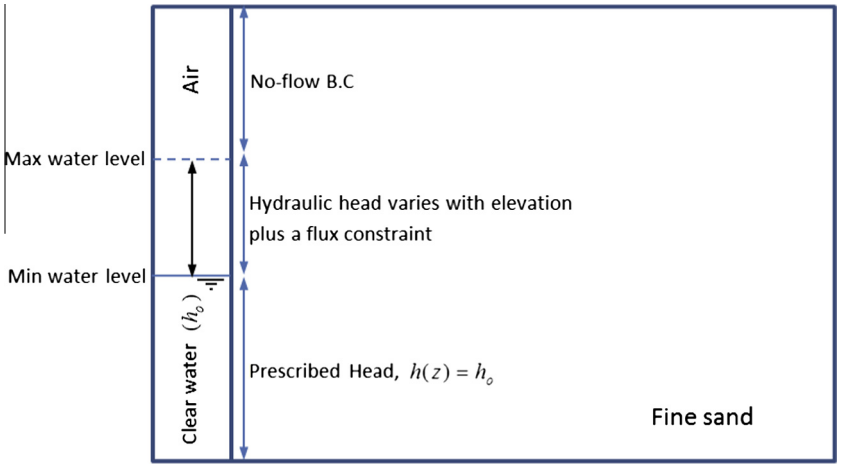

Fig. 4. Hydraulic head combined with flux constraint.

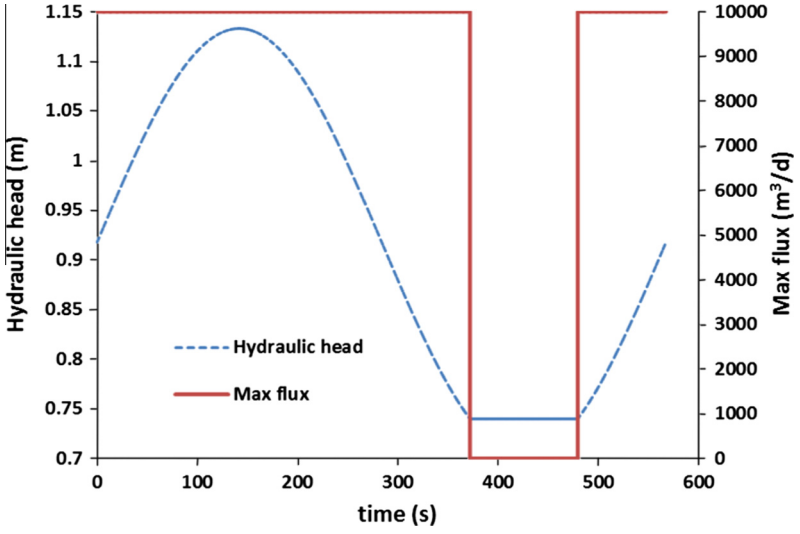

Fig. 5. A sample of hydraulic head time series and flux constraint ($z = 0.74$ m).

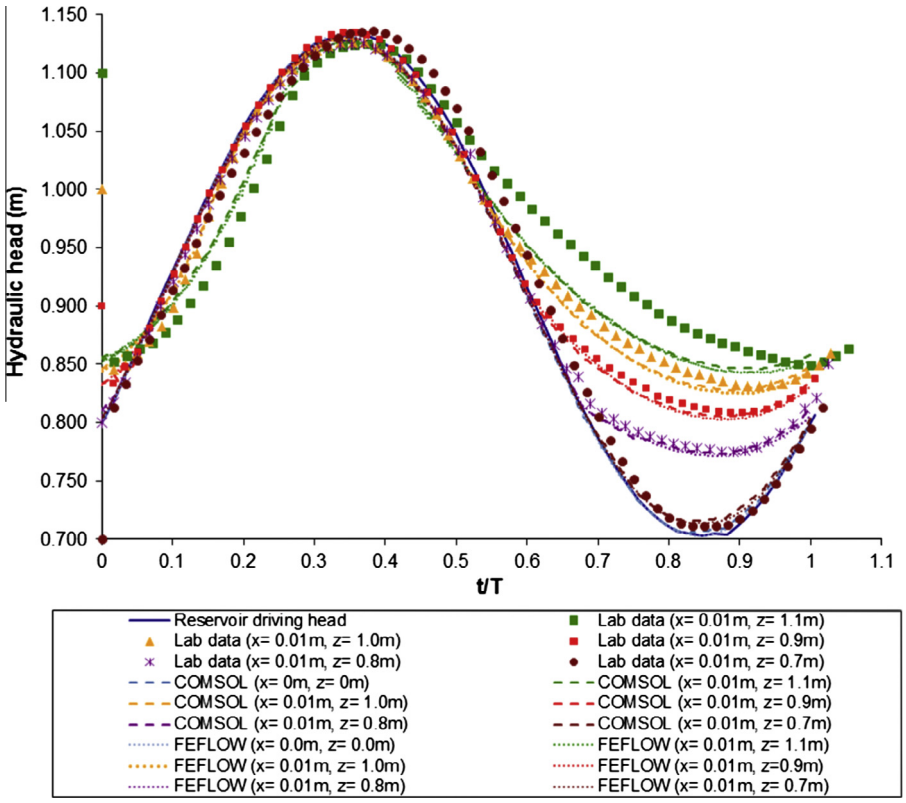

Fig. 6. Comparison of measured and predicted piezometric head time series close to the interface boundary ($x = 0.01$ m) at different elevations ($z = 0.7, 0.8, 0.9, 1.0, 1.1$ m). The symbols show measured laboratory data and curves show numerical modelling results.

harmonic, the piezometric head at higher elevations indicates the influence of the generation of higher harmonic components due to a combination of seepage face formation and the non-linear relationship between moisture content and pore pressure (cf. Eq. (3)).

Typically, the intertidal time series separate from the driving head when the driving head drops below the measurement elevation because of seepage face formation with the falling water level and also due to the draining of pore water which leads to a lower hydraulic conductivity. At $z = 1.1$ m, a significant delay during the rising of driving head is also seen because the sand surrounding the probe becomes partly drained and hence has a lower hydraulic conductivity until it becomes re-saturated and returns to a saturated hydraulic conductivity. The measurements below the low level of driving head are not shown, but they all follow the driving head very closely as shown by the probe at the low level of driving head ($z = 0.7$ m).

The numerical results show that the two different methods applied to simulate seepage face formation produce identical results. In addition, the comparison between the results of both models and laboratory data shows a good agreement for $z \leqslant 0.9$ m. However, at higher elevations there are some obvious discrepancies, especially at the highest elevation ($z = 1.1$ m), where the model underestimates the hydraulic head. This is because model performance in the unsaturated zone will be more sensitive to any uncertainty in the adopted van Genuchten (1980) moisture retention curve parameters (α and β).

Many previous studies (e.g. Lehman et al., 1998; Stauffer and Kinzelbach, 2001; Werner and Lockington, 2003) show that consideration of hysteresis can significantly improve the predictive ability of the Richards' equation under periodic flow conditions. Cartwright et al. (2005) found that using a single non-hysteretic moisture retention curve with $\beta = 3$ captured the observed water table dynamics in periodic sand column experiments. Cartwright (2014) demonstrated that this is due to the fact that the $\beta = 3$ moisture retention curve has a specific moisture capacity ($C_m = d\theta/dH_p$) which more closely resembles the observed moisture-pressure scanning loops compared to the specific moisture capacity found using the first drying curve data ($\beta = 9$).

To examine this further, the model was run using a modified moisture retention curve with $\beta = 3$ that was fit to the ($\beta = 9$) wetting and drying curves (cf. Fig. 7). Note that the wetting curve was estimated based on the observed drying curve ($\beta = 9$) and a

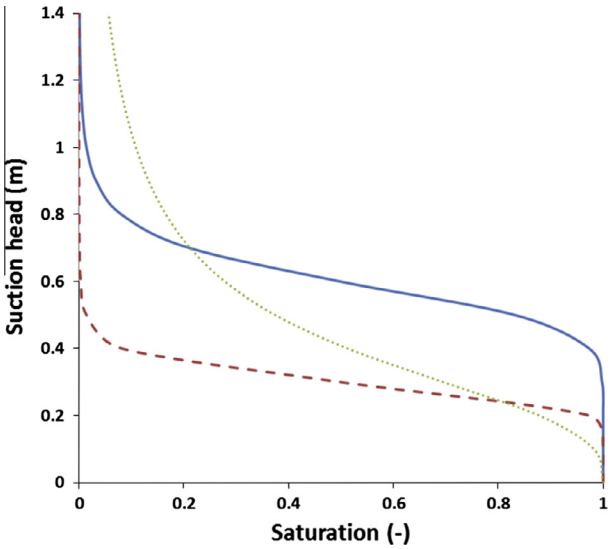

Fig. 7. Drying ($\alpha_d = 1.7$ m^{-1}, $\beta = 9$) (solid line), wetting ($\alpha_w = 3.4$ m^{-1}, $\beta = 9$) (dashed line) and modified ($\alpha = 3$ m^{-1}, $\beta = 3$) (dotted line) retention curves.

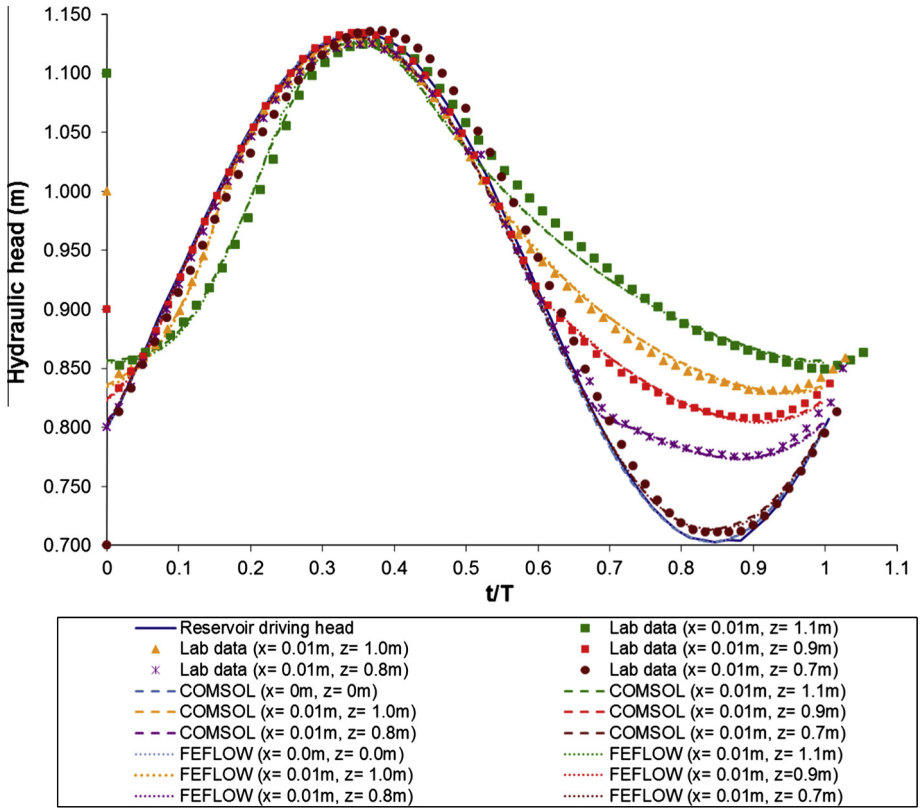

Fig. 8. Comparison of measured and predicted piezometric head time series close to the interface boundary (using modified retention curve with $\alpha = 3\ m^{-1}$ and $\beta = 3$ for numerical models).

hysteresis ratio, $\xi = \alpha_w/\alpha_d = 2$ after Kool and Parker (1987). Fig. 8 shows the new comparison of numerical prediction using $\beta = 3$ with the experimental data for different elevations at $x = 0.01$ m. It is apparent that the modified $\beta = 3$ moisture retention curve significantly improves the numerical results, especially at upper elevations ($z = 1.0, 1.1$ m) in the unsaturated zone where the specific moisture capacity plays a greater role.

Table 2 summarises the harmonic components for laboratory data and numerical results further demonstrating the generation of higher harmonics due to seepage face formation and meniscus suction at the boundary. Above the minimum water elevation ($z = 0.7$ m), the higher order harmonic amplitudes phases are seen to increase with elevation. The maximum ratio of the second harmonic to the fundamental mode is $R_2/R_1 = 0.26$ at ($x = 0.01, z = 1.1$ m). For the third harmonic, the corresponding maximum is $R_3/R_1 = 0.07$ at ($x = 0.01, z = 1.1$ m).

5.2. Pressure head range

Measured and simulated pressure head ranges very close to the boundary ($x = 0.01$ m) are shown in Fig. 9. Since the results of the other simulations (cf. *Range* in Table 2) were almost similar, only the result of FEFLOW simulation with the modified retention curve (i.e. $\alpha = 3\ m^{-1}$ and $\beta = 3$) are shown in this figure. The solid line shows the pressure head range in the reservoir. For elevations below the low water level the head range is similar to reservoir head because of hydrostatic pressure distribution. For $0.7 < z(m) < 0.8$ the head range very close to the reservoir head which means the negative pressure due to meniscuses formation is negligible. For $z > 0.8$ m the pressure head range is separated from the reservoir head because no negative pressure can exist in the reservoir while inside the aquifer at $x = 0.01$ m, formation of meniscuses at the sand surface acts to generate negative pressures and hence the pressure head range reduces for higher elevations. A good agreement between measured and predicted data can be seen in Fig. 9.

5.3. Phase variation of the pressure through various verticals

Fig. 10 shows the comparison of measured and predicted phase lag at $x = 0.01$ m. In both numerical models the best agreement can be obtained by using modified retention curve i.e. van Genuchten parameters of $\alpha = 3\ m^{-1}$ and $\beta = 3$. The phase lag relative to the driving head ($x = 0, z = 0$) is almost zero (i.e. constant phase) below the mean water level ($z = 0.92$ m) indicates hydrostatic behaviour in this range. At higher elevations, the phase lag increases due to non-hydrostatic behaviour in upper elevations which is the result of existence of higher harmonics because of seepage face formation and meniscus suction.

5.4. Mean pressure head profile

Philip (1973) used time averaging of the Boussinesq equation to predict the asymptotic inland overheight of the water table in the absence of meniscus formation and/or seepage formation.

$$\bar{\eta}_\infty = \sqrt{h^2 + \frac{A^2}{2}} - h \approx \frac{A^2}{4h} \tag{10}$$

Cartwright et al. (2003) observed that the asymptotic (landward boundary) value of the time-averaged head profile $\bar{\eta}_\infty$ is less than the 'Boussinesq' value predicted by Philip (1973) (Eq. (10)). The present experiments also showed the same results i.e. a lower measured value of $\bar{h}_\infty = 0.924$ m compared with Philip's

Table 2
Summary of harmonic components.

x (m)	z (m)	$\bar{h}^*$ (m)	$\bar{p}/\rho g$ (m)	h^*_{max} (m)	h^*_{max} (m)	Range (m)	R_1 (m)	ϕ_1 (rad)	R_2 (m)	ϕ_2 (rad)	R_3 (m)	ϕ_3 (rad)
Lab data												
0.00	0.0	0.920	0.920	1.133	0.700	0.433	0.214	2.205	0.005	1.382	0.003	2.175
0.01	0.7	0.922	0.222	1.125	0.712	0.420	0.214	2.230	0.001	0.587	0.002	3.526
0.01	0.8	0.941	0.141	1.125	0.775	0.350	0.186	2.238	0.014	4.525	0.007	3.444
0.01	0.9	0.951	0.051	1.126	0.808	0.326	0.167	2.243	0.026	4.120	0.007	2.968
0.01	1.0	0.964	−0.036	1.132	0.831	0.295	0.152	2.350	0.031	4.040	0.004	4.498
0.01	1.1	0.968	−0.132	1.134	0.849	0.276	0.136	2.499	0.036	4.224	0.009	5.877
FEFLOW (α = 1.7, β = 9.0)												
0.00	0.0	0.918	0.918	1.133	0.703	0.430	0.215	1.593	0.000	1.574	0.000	1.563
0.01	0.7	0.920	0.220	1.131	0.714	0.417	0.211	1.596	0.002	3.048	0.001	1.585
0.01	0.8	0.933	0.133	1.131	0.772	0.359	0.187	1.603	0.018	3.096	0.009	1.493
0.01	0.9	0.946	0.046	1.130	0.803	0.328	0.166	1.633	0.024	2.944	0.005	1.269
0.01	1.0	0.955	−0.045	1.130	0.825	0.305	0.152	1.693	0.028	2.910	0.003	2.806
0.01	1.1	0.957	−0.143	1.128	0.842	0.285	0.136	1.797	0.031	3.093	0.008	4.332
COMSOL (α = 1.7, β = 9.0)												
0.00	0.0	0.918	0.918	1.133	0.703	0.429	0.215	2.148	0.000	2.180	0.000	1.586
0.01	0.7	0.919	0.219	1.131	0.712	0.419	0.210	2.151	0.002	4.263	0.001	3.160
0.01	0.8	0.933	0.133	1.130	0.772	0.359	0.186	2.157	0.018	4.220	0.009	3.149
0.01	0.9	0.946	0.046	1.130	0.803	0.327	0.166	2.186	0.024	4.071	0.005	2.880
0.01	1.0	0.955	−0.045	1.129	0.826	0.303	0.152	2.248	0.028	4.038	0.002	4.499
0.01	1.1	0.957	−0.143	1.125	0.844	0.282	0.135	2.365	0.031	4.297	0.007	0.044
FEFLOW (α = 3.0, β = 3.0)												
0.00	0.0	0.918	0.918	1.133	0.703	0.430	0.215	1.593	0.000	1.574	0.000	1.563
0.01	0.7	0.920	0.220	1.131	0.714	0.417	0.210	1.597	0.002	2.983	0.001	1.571
0.01	0.8	0.933	0.133	1.131	0.773	0.358	0.186	1.608	0.019	3.038	0.010	1.408
0.01	0.9	0.947	0.047	1.130	0.804	0.326	0.164	1.661	0.027	2.802	0.006	1.103
0.01	1.0	0.958	−0.042	1.130	0.829	0.301	0.148	1.763	0.034	2.771	0.004	2.686
0.01	1.1	0.965	−0.135	1.127	0.855	0.272	0.126	1.936	0.039	3.029	0.011	4.001
COMSOL (α = 3.0, β = 3.0)												
0.00	0.0	0.918	0.918	1.133	0.703	0.430	0.215	2.148	0.000	2.360	0.000	2.102
0.01	0.7	0.919	0.219	1.131	0.713	0.418	0.210	2.152	0.002	4.199	0.001	3.242
0.01	0.8	0.933	0.133	1.131	0.774	0.356	0.185	2.164	0.019	4.151	0.010	3.075
0.01	0.9	0.947	0.047	1.130	0.805	0.325	0.163	2.215	0.027	3.928	0.006	2.761
0.01	1.0	0.958	−0.042	1.129	0.830	0.299	0.147	2.320	0.034	3.903	0.004	4.444
0.01	1.1	0.965	−0.135	1.125	0.856	0.269	0.124	2.502	0.039	4.174	0.011	5.753

Mean water head ($\bar{h}^*$), mean pressure head ($\bar{p}/\rho g$), maximum water elevation (h^*_{max}), minimum water elevation (h^*_{min}), pressure head range (*Range*), first harmonic amplitude (R_1), first harmonic phase (ϕ_1), second harmonic amplitude (R_2), second harmonic phase (ϕ_2), third harmonic amplitude (R_3), third harmonic phase (ϕ_3).

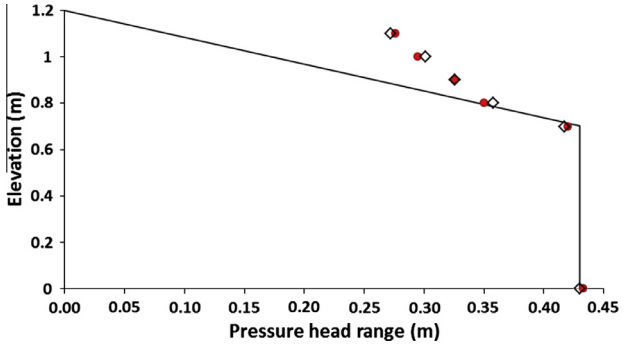

Fig. 9. Comparison of measured and predicted pressure head range at x = 0.01 m. Lab data (solid circles) and numerical results of FEFLOW using modified retention curve (i.e. α = 3 m^{-1} and β = 3) (open diamonds). Solid line shows the pressure head range in the reservoir.

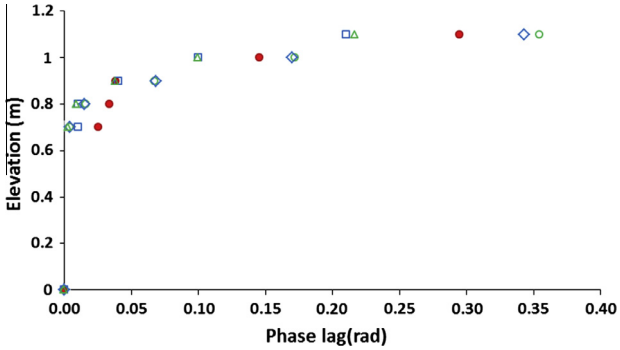

Fig. 10. Comparison of measured and predicted phase lag at x = 0.01 m. Lab data (solid circles) and FEFLOW and COMSOL results with α = 1.7 m^{-1} and β = 9 open squares and triangles, respectively. FEFLOW and COMSOL results with α = 3 m^{-1} and β = 3 open diamonds and circles, respectively.

$\bar{h}_\infty = \sqrt{d^2 + \frac{1}{2}A^2} = 0.932$ m, corresponding to a measured over-height of 4 mm and a predicted of 12 mm. Knight (1982) showed Philip's result is valid even for non-shallow aquifer, hence this difference is likely due to negative pressure above the driving head and capillary fringe effects which are not accounted by Philip's theory.

The time-averaged pressure head distribution above the low water level without considering the capillarity effects can be expressed as (see Appendix A for details),

$$\frac{\bar{p}}{\rho g} = \frac{1}{\pi}\left[(d-z)\cos^{-1}\left(\frac{z-d}{A}\right) + A\sqrt{1-\left(\frac{z-d}{A}\right)^2}\right] \quad (11)$$

Fig. 11 compares the measured and predicted time-averaged pressure head at different elevations at x = 0.01 m. For clarity, only the FEFLOW results using modified retention curve (i.e. α = 3 m^{-1} and β = 3) are shown in the figure. The results of other simulations show the same trend and they are summarised in Table 2 (cf. $\bar{p}/\rho g$). The time-averaged pressure head distribution calculated

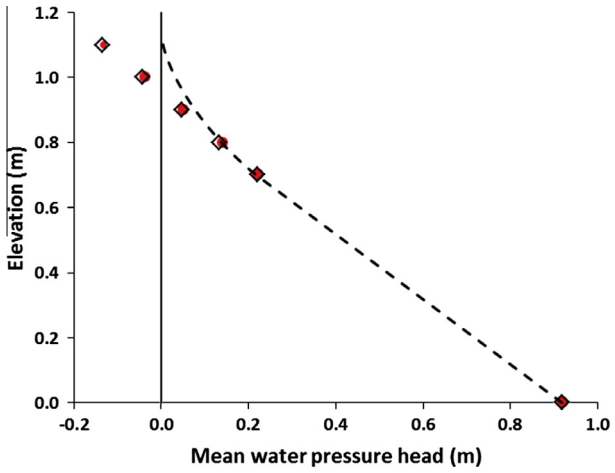

Fig. 11. Comparison of measured and predicted mean pressure head profile at $x = 0.01$ m. Lab data (solid circles) and numerical results of FEFLOW using modified retention curve (i.e. $\alpha = 3\ m^{-1}$ and $\beta = 3$) (open diamonds). The dashed line shows the theoretical profile calculated by Eq. (11). Solid line represents the vertical sand interface.

by Eq. (11) is also shown in the figure as a reference. A good agreement between model results and laboratory data can be seen in this figure.

As expected, the mean water pressure head is hydrostatic below the minimum water level ($z \leqslant 0.7$ m). For $0.7 < z(m) < 0.8$ the trend still follows the theoretical curve suggesting that the meniscuses and capillary effects are not significant in this range due to the presence of a seepage face during the falling stage of driving head. For $z > 0.8$ m, the mean water pressure head is lower than the theoretical curve demonstrating the significance of negative pressures at the boundary (i.e. meniscus formation and capillarity effects).

6. Conclusion

A laboratory sand flume has been used to observe the piezometric head in an idealised unconfined aquifer bordering a tidal (simple harmonic) reservoir with a vertical interface. The data demonstrate the influence of seepage face and meniscus formation at the boundary which lead to the generation of higher harmonics in the pore pressure time series at locations above the water table. The data also show that the formation of meniscuses and capillary suction has a significant effect on reduction of mean pressure head and pressure head range in upper elevation above minimum water level where located in unsaturated zone and have lower hydraulic conductivity related to saturated part. At higher elevations, the phase lag related to the tide is also increased due to non-hydrostatic behaviour which is the result of existence of higher harmonics because of seepage face formation and meniscus suction. The laboratory data indicate that the seepage face formation and capillary suction due to meniscuses play an important role in ground water flow and should be considered in the numerical models by using unsaturated flow models.

The experimental data was then used to evaluate the predictive capabilities of a numerical solution of the Richards' equation. Two approaches to the boundary condition were evaluated. The first method used a mixed (Cauchy) type boundary condition with appropriate logic statements to switch between a Dirichlet boundary condition below the ocean level and in the seepage face and a Neumann boundary condition above of the water table exit point. The second method was a combination of a prescribed head and the flux constraint condition to activate a Dirichlet boundary condition below the ocean level and along the seepage face and a Neumann boundary condition above the exit point. The results show that both methods were equal in capturing the influence of seepage face and meniscus formation on the pressure along the boundary.

The comparison between the simulated and measured pressure head distribution along the boundary revealed significant discrepancies, especially in higher elevations (located in the unsaturated zone). These discrepancies were overcome by adopting a modified moisture retention curve with a specific moisture capacity ($C_m = d\theta/dH_p$) more closely related to the moisture-pressure scanning loops observed by Cartwright (2014) using the same sand type.

In terms of the mean pressure head profile near the boundary, the simulated results are in a good agreement with the laboratory data. The results also show the effect of capillary suction and meniscuses formation in reducing the mean pressure head in upper elevations near the boundary. In addition, comparison of harmonic components of laboratory data and numerical results show the ability of numerical models to reproduce the generation of higher harmonic in hydraulic head time series in upper elevation located in capillary fringe.

It is noted that the present study considers the simple case of a vertical boundary. However, for natural systems such as beaches and river banks, the interface is generally sloped. The methods demonstrated in this paper to simulate the effects of seepage face and meniscus formation can readily be applied on sloped surface and is the focus of ongoing work.

The interaction of surface and subsurface water at the beach face plays a vital role in changing the hydraulic gradients and controlling the in/exfiltration across the interface. In/exfiltration across the beach face is linked to both sediment transport (e.g. Elfrink and Baldock, 2002) and also contaminant transport and saltwater intrusion (e.g. Xin et al., 2010). The data and modelling approaches discussed in this paper will thus provide some useful insights into more accurate modelling of these types of problems.

Acknowledgements

The first author has been supported by Griffith University International Postgraduate Research Scholarship (GUIPRS) and Griffith University Postgraduate Research Scholarship (GUPRS).

Appendix A. Capillary free time-averaged pressure head profile

Below the low level of driving head the time-averaged piezometric head in the reservoir is d. Above the low level of driving head, in a capillarity free scenario (zero pressure at all points above water), it is given by

$$\bar{h}^* = \frac{1}{T}\int_{t_u}^{t_d}(d + A\cos\omega t)dt + [T - (t_d - t_u)]z \tag{A1}$$

where $t_u(z)$, respectively $t_d(z)$ are the time of zero upcrossing and downcrossing for the water surface through the level z, i.e., $t_u = -(T/2\pi)\cos^{-1}(z/A)$ and $t_d = (T/2\pi)\cos^{-1}(z/A)$ $t_d = (T/2\pi)\cos^{-1}(z/A)$. This leads to

$$\bar{h}^* = \frac{1}{\pi}\int_{\omega t=0}^{\cos^{-1}\frac{z-d}{A}}(d + A\cos\omega t)d\omega t + \left[1 - \frac{1}{\pi}\cos^{-1}\left(\frac{z-d}{A}\right)\right]d \tag{A2}$$

$$\bar{h}^* = z + \frac{1}{\pi}\left[(d-z)\cos^{-1}\left(\frac{z-d}{A}\right) + A\sqrt{1 - \left(\frac{z-d}{A}\right)^2}\right] \tag{A3}$$

and the corresponding mean pressure head

$$\frac{\bar{p}}{\rho g} = \frac{1}{\pi}\left[(d-z)\cos^{-1}\left(\frac{z-d}{A}\right) + A\sqrt{1 - \left(\frac{z-d}{A}\right)^2}\right] \tag{A4}$$

References

Ataie-Ashtiani, B., Volker, R.E., Lockington, D.A., 1999. Numerical and experimental study of seepage in unconfined aquifers with a periodic boundary condition. J. Hydrol. 222 (1–4), 165–184, 13.

Baird, A.J., Horn, D.P., Mason, T.E., 1998. Validation of a Boussinesq model of beach ground water behaviour. Mar. Geol. 148, 55–69.

Barry, D.A., Barry, S.J., Parlange, J.-Y., 1996. Capillarity correction to Periodic solutions of the shallow flow approximation. In: Pattiaratchi, C.B. (Ed.), Mixing in Estuaries and Coastal Seas, Coastal and Estuarine Studies. AGU, Washington, DC, pp. 496–510.

Bradshaw, M.P., 1974. High frequency water table fluctuations and mass movement on sandy beaches. BA Honours Thesis, Department of Geography, Australian National University, p. 122.

Cartwright, N., 2014. Moisture-pressure dynamics above an oscillating water table. J. Hydrol. 512, 442–446.

Cartwright, N., Nielsen, P., 2001a. Groundwater dynamics and salinity in beaches. In: Proceedings of Coasts and Ports 2001, 15th Australasian Coastal and Ocean Engineering Conference. Gold Coast, Australia, pp. 441–446.

Cartwright, N., Nielsen, P., 2001b. Groundwater dynamics and salinity in coastal barriers'. Proc. SWICA-M3, 1st Intl. Conf. on Saltwater Intrusion and Coastal Aquifers – Monitoring, Modelling and Management (Essauira, Morocco), April 23–25, 2001, CD-ROM.

Cartwright, N., Nielsen, P., 2003. Dynamics of the salt–freshwater mixing zone in ocean beaches. In: Proceedings of the Second International Conference on Saltwater Intrusion and Coastal Aquifers, Mé rida, Mexico, CD-ROM.

Cartwright, N., Nielsen, P., Jessen, O.Z., 2002. Swash zone and near-shore water table dynamics, in: Proc. 28th Intl. Conf. on Coastal Engineering, ASCE, (Cardiff, Wales), July 7–12, 2002, pp. 1006–1015.

Cartwright, N., Nielsen, P., Dunn, S.L., 2003. Water table waves in an unconfined aquifer: experiments and modeling. Water Resour. Res. 39 (12), 1330–1342.

Cartwright, N., Li, L., Nielsen, P., 2004a. Response of the salt–freshwater interface in a coastal aquifer to a wave induced groundwater pulse: field observations and modelling. Adv. Water Resour. 27, 297–303.

Cartwright, N., Nielsen, P., Li, L., 2004b. The influence of offshore storm waves on groundwater dynamics and salinity in a sandy beach. In: Proceedings of the 29th International Conference on Coastal Engineering. World Scientific, Singapore, pp. 1841–1850.

Cartwright, N., Nielsen, P., Perrochet, P., 2005. The influence of capillarity on a simple harmonic oscillating water table: sand column experiments and modelling. Water Resour. Res. 41 (8), W08416.

Cartwright, N., Baldock, T.E., Nielsen, P., Jeng, D.S., Tao, L., 2006. Swash-aquifer interaction in the vicinity of the water table exit point on a sandy beach. J. Geophys. Res. (Oceans) 111, C09035. http://dx.doi.org/10.1029/2005JC003149.

Chui, T.F.M., Freyberg, D.L., 2009. Implementing hydrologic boundary conditions in a multiphysics model. Hydrol. Eng. 14 (12), 1374–1377.

Clement, T.P., Wise, W.R., Molz, F.J., 1994. A physically based, two-dimensional, finite-difference algorithm for modelling variably saturated flow. J. Hydrol. 161, 71–90.

COMSOL, 2013. COMSOL: Subsurface Flow Module User's Guide Version 4.3b, p. 240.

Cooley, R.L., 1983. Some new procedures for numerical solution of variably saturated flow problems. Water Resour. Res. 19, 1271–1285.

Dracos, T., 1963. Ebene nichtstationäre Grundwasserabflüsse mit freier Oberfläche. Mitteilungen Versuchsanstalt fur Wasserbau und Erdbau, Eidgenoss tech Hochsch, Zürich, 114.

Elfrink, B., Baldock, T.E., 2002. Hydrodynamics and sediment transport in the swash zone: a review and perspectives. Coast. Eng. 45, 149–167.

Emery, K.O., Foster, J.F., 1948. Water tables in marine beaches. J. Mar. Res. 7, 644–654.

Ericksen, N.J., 1970. Measurement of tide induced change to water table profiles in coarse and fine sand beaches along Pegasus Bay, Canterbury. Earth Sci. J. 4 (1), 24–31.

FEFLOW, 2012. Finite Element Subsurface Flow and Transport Simulation System, User Manual Version 6.0, p. 116.

Grant, U.S., 1946. Effects of groundwater table on beach erosion. Geol. Soc. Am. Bull. 57, 1952 (abstract).

Grant, U.S., 1948. Influence of the water table on beach aggradation and degradation. J. Mar. Res. 7, 655–660.

Hegge, B.J., Masselink, G., 1991. Groundwater-table responses to wave run-up: an experimental study from Western Australia. J. Coastal Res. 7 (3), 623–634.

Isla, F.I., Bujalesky, G.G., 2005. Groundwater dynamics on macrotidal gravel beaches of Tierra del Fuego, Argentina. J. Coast. Res. 21 (1), 65–72.

Kang, H.-Y., Nielsen, P., Hanslow, D., 1994. Water table overheight due to wave runup on a sandy beach. In: Proceedings of the 24th International Conference on Coastal Engineering. American Society of Civil Engineers, New York, pp. 2115–2124.

Knight, J.H., 1982. Steady periodic flow through a dam. Water Resour. Res. 17 (4), 1222–1224.

Kool, J.B., Parker, J.C., 1987. Development and evaluation of closed-form expressions for hysteretic soil hydraulic properties. Water Resour. Res. 23 (1), 105–114.

Lanyon, J.A., Eliot, I.G., Clarke, D.J., 1982. Observations of shelf waves and bay sieches from tidal and beach groundwater records. Mar. Geol. 49, 23–42.

Lehman, P., Stauffer, F., Hinz, C., Dury, O., Flühler, H., 1998. Effect of hysteresis on water flow in a sand column with a fluctuating capillary fringe. J. Contam. Hydrol. 33 (1–2), 81–100.

Lewandowski, A., Zeidler, R.B., 1978. Beach ground-water oscillations. In: Proceedings of the 16th Conference on Coastal Engineering, pp. 2051–2065.

Li, L., Barry, D.A., Pattiaratchi, C.B., 1997. Numerical modelling of tide-induced beach water table fluctuations. Coast. Eng. 30 (1/2), 105–123.

Li, L., Barry, D.A., Stagnitti, F., Parlange, J.-Y., 2000. Groundwater waves in a coastal aquifer: a new governing equation including vertical effects and capillarity. Water Resour. Res. 36 (2), 411–420.

Li, L., Barry, D.A., Pattiaratchi, C.B., Masselink, G., 2002. BeachWin: modelling groundwater effects on swash sediment transport and beach profile changes. Environ. Model. Softw. 17, 313–320.

Liggett, J.A., Liu, P.L.-F., 1983. The Boundary Integral Equation Method for Porous Media Flow. George Allen and Unwin, London.

Neuman, S.P., 1973. Saturated–unsaturated seepage by finite elements. J. Hydraul. Div. Am. Soc. Civ. Eng. 99 (Hy12), 2233–2250.

Nielsen, P., 1990. Tidal dynamics of the water table in beaches. Water Resour. Res. 26, 2127–2134.

Nielsen, P., 1999. Groundwater dynamics and salinity in coastal barriers. J. Coastal Res. 15 (3), 732–740.

Nielsen, P., Perrochet, P., 2000. Water table dynamics under capillary fringes: experiments and modeling. Adv. Water Resour. 23 (1), 503–515.

Nielsen, P., Turner, I., 2000. Groundwater waves and water exchange in beaches. In: Paper Presented at Proc. 27th Intl. Conf. on Coastal Engineering, ASCE, Sydney, Australia.

Nielsen, P., Voisey, C.J., 1998. Water table heights and salinity in coastal barriers: field measurements. Research Report No. CH49/98, Department of Civil Engineering, The University of Queensland.

Nielsen, P., Aseervatham, A.M., Fenton, J.D., Perrochet, P., 1997. Groundwater waves in aquifers of intermediate depths. Adv. Water Resour. 20 (1), 37–43.

Philip, J.R., 1973. Periodic non-linear diffusion: an integral relation and its physical consequences. Aust. J. Phys. 26, 513–519.

Richards, L.A., 1931. Capillary conduction of liquids through porous mediums. Physics 1 (5), 318–333.

Robinson, C., Gibbes, B., Li, L., 2006. Driving mechanisms for groundwater flow and salt transport in a subterranean estuary. Geophys. Res. Lett. 33 (3), L03402. http://dx.doi.org/10.1029/2005GL025247.

Silliman, S.E., Berkowitz, B., Simunek, J., van Genuchten, M.Th., 2002. Fluid flow and solute migration within the capillary fringe. Ground Water 40 (1), 76–84.

Simpson, M.J., Clement, T.P., Gallop, T.A., 2003. Laboratory and numerical investigation of flow and transport near a seepage-face boundary. Groundwater 41 (5), 690–700.

Stauffer, F., Kinzelbach, W., 2001. Cyclic hysteretic flow in porous medium column: model, experiment, and simulations. J. Hydrol. 240 (3–4), 264–275.

Turner, I.L., 1993a. The total water content of sandy beaches. J. Coast. Res. 15, 11–26.

Turner, I.L., 1993b. Water table outcropping on macro-tidal beaches: a simulation model. Mar. Geol. 115, 227–238.

Turner, I.L., 1995. Simulating the influence of groundwater seepage on sediment transported by the sweep of the swash zone across the intertidal profile of macrotidal beaches. Mar. Geol. 125, 153–174.

Turner, I.L., 1998. Monitoring groundwater dynamics in the littoral zone at seasonal, storm, tide and swash frequencies. Coast. Eng. 35, 1–16.

Turner, I.L., Acworth, R.I., 2004. Field measurements of beachface salinity structure using cross-borehole resistivity imaging. J. Coastal Res. 20 (3), 753–760.

Turner, I.L., Masselink, G., 1998. Swash infiltration–exfiltration and sediment transport'. J. Geophys. Res. 103 (C13), 30813–30824.

Turner, I.L., Nielsen, P., 1997. Rapid water table fluctuations within the beachface: implications for swash zone sediment mobility? Coast. Eng. 32, 45–59.

Turner, I.L., Coates, B.P., Acworth, R.I., 1997. Tides, waves and the super-elevation of groundwater at the coast. J. Coastal Res. 13–1, 46–60.

van Genuchten, M.T., 1980. A closed form equation for predicting the hydraulic conductivity of unsaturated soils. Soil Sci. Soc. Am. J. 44, 892–898.

Voss, C.I., 1984. SUTRA: a finite element simulation model for saturated–unsaturated, fluid-density dependent ground-water flow with energy transport or chemically reactive single species solute transport. US Geological Survey, National Centre, Reston, VA.

Waddell, E., 1973. Dynamics of swash and implications to beach response. Technical Report 139, Coastal Studies Institute, Louisiana State University, Baton Rouge.

Waddell, E., 1976. Swash-groundwater-beach profile interactions. In: Davis, R.A., Etherington, R.L. (Eds.), Beach and Nearshore Sedimentation, vol. 24. Society of Economic and Paleontological Mineralogists Special Publication, pp. 115–125.

Waddell, E., 1980. Wave forcing of beach groundwater. In: Proceedings of the 17th International Conference on Coastal Engineering, pp. 1436–1452.

Werner, A.D., Lockington, D.A., 2003. Influence of hysteresis on tidal capillary fringe dynamics in a well-sorted sand. Adv. Water Resour. 26, 1199–1204.

Xin, P., Robinson, C., Li, L., Barry, D.A., Bakhtyar, R., 2010. Effects of wave forcing on a subterranean estuary. Water Resour. Res. 46, W12505, 10.1029/2010WR009632.